

UAV-Enabled Communication Using NOMA

Ali A. Nasir, Hoang D. Tuan, Trung Q. Duong and H. Vincent Poor

Abstract

Unmanned aerial vehicles (UAVs) can be deployed as flying base stations (BSs) to leverage the strength of line-of-sight connections and effectively support the coverage and throughput of wireless communication. This paper considers a multiuser communication system, in which a single-antenna UAV-BS serves a large number of ground users by employing non-orthogonal multiple access (NOMA). The max-min rate optimization problem is formulated under total power, total bandwidth, UAV altitude, and antenna beamwidth constraints. The objective of max-min rate optimization is non-convex in all optimization variables, i.e. UAV altitude, transmit antenna beamwidth, power allocation and bandwidth allocation for multiple users. A path-following algorithm is proposed to solve the formulated problem. Next, orthogonal multiple access (OMA) and dirty paper coding (DPC)-based max-min rate optimization problems are formulated and respective path-following algorithms are developed to solve them. Numerical results show that NOMA outperforms OMA and achieves rates similar to those attained by DPC. In addition, a clear rate gain is observed by jointly optimizing all the parameters rather than optimizing a subset of parameters, which confirms the desirability of their joint optimization.

Index Terms

A. A. Nasir is with the Department of Electrical Engineering, King Fahd University of Petroleum and Minerals (KFUPM), Dhahran, Saudi Arabia (Email: anasir@kfupm.edu.sa).

H. D. Tuan is with the School of Electrical and Data Engineering, University of Technology Sydney, Broadway, NSW 2007, Australia (email: Tuan.Hoang@uts.edu.au).

T. Q. Duong is with Queen's University Belfast, Belfast BT7 1NN, UK (email: trung.q.duong@qub.ac.uk)

H. V. Poor is with the Department of Electrical Engineering, Princeton University, Princeton, NJ 08544, USA (e-mail: poor@princeton.edu).

Unmanned aerial vehicle (UAV), non-orthogonal multiple access (NOMA), orthogonal multiple access (OMA), dirty paper coding (DPC), non-convex optimization, throughput.

I. INTRODUCTION

Unmanned aerial vehicles (UAVs) can assist normal communication networks by acting as flying base stations (UAV-BSs) and taking care of traffic demand in exceptional situations, e.g., sports events, concerts, disaster position, military situations, traffic congestion, etc. [1]–[6]. UAVs can also function as temporary hotspots or relay nodes for connections between the safe area and disaster areas [7]–[9]. Ground users served by the UAV-BSs can expect line-of-sight (LoS) air-to-ground communication. Thus, UAV-enabled communication can be efficient in supporting the coverage and throughput of wireless communications [10], [11].

UAV-enabled communication networks have recently gained significant interests and are actively investigated in open literature. Thanks to the flexibility of UAV deployment, the coverage area, throughput, and energy efficiency of UAV-enabled communication can be improved by UAV placement [12]–[14], beamwidth control [15], [16], and power allocation [1], [17], [18].

Unlike conventional cellular communication, which operates in a rich scattering environment that supports multi-antenna array transmission for spatial diversity, UAV-enabled downlink communication exhibits much poorer scattering and as such a single-antenna UAV is most desired. To be served by the same UAV over the same time, multiple users must share the communication bandwidth. Usually each user is assigned an individual bandwidth channel so its achievable rate is very sensitive to the number of users sharing the same bandwidth. Naturally one may think to assign a bandwidth channel to a group users but this would be not efficient because it is conventionally known that over the same transmission bandwidth, the downlink communication is only efficient when the number of transmit antennas is not less than the number of served users. Meanwhile, non-orthogonal multiple access (NOMA) is known to simultaneously serve multiple users in non-orthogonal resources, by

separating the users in the power domain [19], [20]. NOMA can improve the achievable rate of far users (who receive lower received signal power) by allowing the near-by users (who receive higher received signal power) to access the information intended for the far users [21], [22].

There are quite a few recent studies that have considered the use of NOMA to improve the performance of UAV-enabled communication system. In [23], the authors considered a UAV-BS to communicate with two ground users using NOMA and investigated their outage probability. In [24], the authors considered a multi-antenna UAV-BS to generate directional beams and served multiple users to maximize their outage sum rates by using NOMA and beam scanning. In [25], the authors employed a UAV system and NOMA to optimize power allocation and UAV altitude to maximize sum-rate for two users [25]. However, in order to achieve the maximum rate gains from UAV-enabled communication, it is important to jointly optimize multiple relevant parameters, e.g., UAV altitude, antenna beamwidth, power allocation and bandwidth allocation. To the best authors' knowledge, this important problem, with a NOMA setting, is still unsolved.

In this article, we consider a multiuser communication system, in which a single-antenna UAV-BS serves a large number of ground users by employing NOMA. We jointly optimize multiple parameters, e.g., the UAV's flying altitude, transmit antenna beamwidth, and the amount of power and bandwidth allocated to multiple users. Our objective is to solve the max-min rate optimization problem under total power, total bandwidth, UAV altitude and antenna beamwidth constraints. The objective function is non-convex in all optimization variables, i.e., power, bandwidth, altitude, and beamwidth. In addition, it is also challenging to handle the coverage constraint, which is dependent nonlinearly on the beamwidth and UAV altitude. We tackle these challenges by using inner convex approximations and propose a path-following algorithm to solve the problem. We also formulate orthogonal multiple access (OMA) and dirty paper coding (DPC)-based max-min rate optimization problems and develop path-following algorithms to solve them. Numerical results show that NOMA

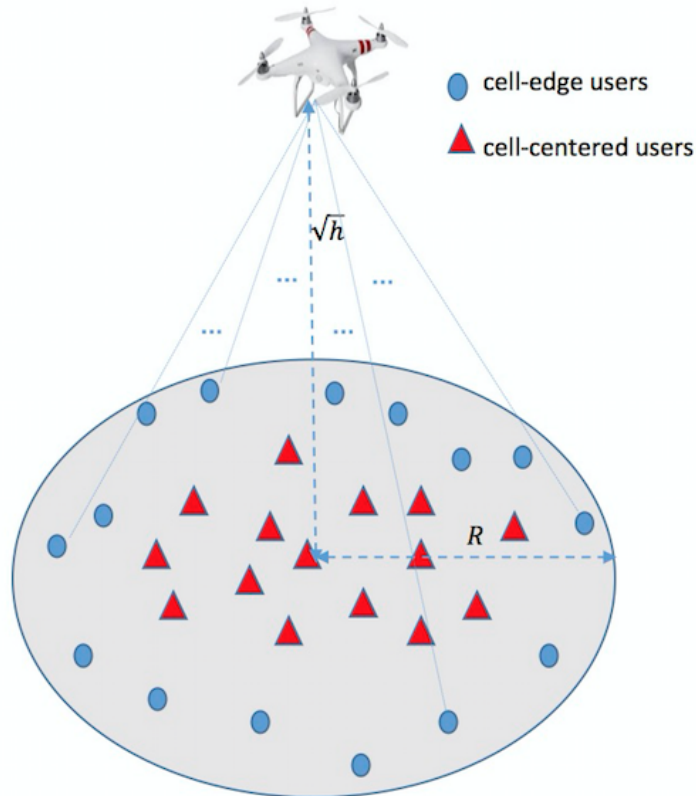


Fig. 1. A system model showing UAV-BS and the ground users.

outperforms OMA and achieves rates similar to those attained by DPC. In addition, we observe a clear rate gain by jointly optimizing all the parameters rather than optimizing subset of parameters, which emphasize the need of their joint optimization.

Organization: The paper is organized as follows. Section II presents the formulation of max-min rate optimization problems. Section III describes algorithms to solve the formulated problems. Section IV evaluates the performance of our proposed algorithms using numerical examples. Finally, Section V concludes the paper.

II. SYSTEM MODEL AND PROBLEM STATEMENT

Let us consider that a certain out-door location (stadium, traffic jam, concert, etc.) is served by a single-antenna UAV as depicted in Fig. 1. We assume that there are K ground users in the

location, such that $K/2$ users, $k \in \{1, \dots, K/2\}$, are located in closer vicinity (in terms of Euclidean distance) of the UAV, and are called “near users” or “cell-centered users”. The remaining $K/2$ users, $k \in \{K/2 + 1, \dots, K\}$ are located relatively at farther distances, and are called “far users” or “cell-edge users”. The UAV can employ NOMA to pair each near user with each of the far users.

Let θ be the squared antenna beamwidth, h be the squared UAV altitude (or UAV height above ground), which must satisfy the coverage condition

$$R \leq \sqrt{h} \tan \sqrt{\theta}, \quad (1)$$

where R is the radius of the coverage, so all users are located inside the coverage area. Note that we have to use \sqrt{h} and $\sqrt{\theta}$ for the UAV altitude and its antenna beamwidth, respectively, as it will later on simplify the handling of non-convex coverage constraint (1). Let g denote the channel power gain at a reference distance of 1 m, $z_k = (x_k, y_k)$ denote the coordinates of user k and $z_u = (x_u, y_u)$ denote the location of the UAV projected on the horizontal ground plane. The channel power gain between the UAV and user k is given by

$$\tilde{h}_k(h, \theta) = \frac{g}{\theta(\|z_k - z_u\|^2 + h)}, \quad (2)$$

which assumes a free-space path loss model with path-loss exponent 2 since users are dominated by LoS links [24], [26].

Let \mathcal{B} be the total available bandwidth, which can be optimally divided among the near-by users $k \in \{1, \dots, K/2\}$, such that the bandwidth allocated for user k can be written as

$$w_k = \tau_k \mathcal{B}, \quad k \in \{1, \dots, K/2\} \quad (3)$$

where $0 \leq \tau_k \leq 1$ is the fraction of the bandwidth allocated to the user k . Accordingly, each near-by user k is “assigned” a far-user $j(k) = k + K$ to share the bandwidth w_k .

There are a couple of transmission techniques to improve the multi-user rates. In the following, we will formulate the multi-user rate max-min optimization problem for NOMA, DPC, and OMA.

A. NOMA Problem Formulation

To make the rate functions more appealing, we use (2) and introduce the definitions

$$d_k = \|z_k - z_u\|^2, k = 1, \dots, K.$$

NOMA allows user k to decode the information intended for user $j(k)$ to cancel user $j(k)$'s interference in decoding the information intended for it. Assuming additive white Gaussian noise (AGWN) channel, the achievable rate in nats/sec/Hz of user $k \in \{1, 2, \dots, K/2\}$, is given by

$$\begin{aligned} r_k(\boldsymbol{\tau}, \mathbf{p}, h, \theta) &= \tau_k \ln \left(1 + \frac{p_k \bar{h}_k(h, \theta)}{\sigma_B \tau_k} \right) \\ &= \tau_k \ln \left(1 + \frac{gp_k}{\sigma_B \tau_k \theta (d_k + h)} \right), k \in \{1, 2, \dots, K/2\} \end{aligned} \quad (4)$$

where $\sigma_B = \sigma^2 \mathcal{B}$ with the noise power density σ^2 , so $\sigma_B \tau_k$ is the noise power over the bandwidth $\tau_k \mathcal{B}$, p_k is the power of signal carrying the information intended for it, $\boldsymbol{\tau} \triangleq (\tau_1, \dots, \tau_{K/2})$, and $\mathbf{p} \triangleq (p_1, \dots, p_K)$.

The achievable rate of user $j(k)$ in nats/sec/Hz is given by

$$r_{j(k)}(\boldsymbol{\tau}, \mathbf{p}, h, \theta) = \min \{r_{j(k)}^1(\boldsymbol{\tau}, \mathbf{p}, h, \theta), r_{j(k)}^2(\boldsymbol{\tau}, \mathbf{p}, h, \theta)\} \quad (5)$$

where

$$\begin{aligned} r_{j(k)}^2(\boldsymbol{\tau}, \mathbf{p}, h, \theta) &= \tau_k \ln \left(1 + \frac{p_{j(k)} \bar{h}_{j(k)}(h, \theta)}{\sigma_B \tau_k + p_k \bar{h}_{j(k)}(h, \theta)} \right) \\ &= \tau_k \ln \left(1 + \frac{gp_{j(k)}}{\sigma_B \tau_k \theta (d_{j(k)} + h) + gp_k} \right), k \in \{1, 2, \dots, K/2\} \end{aligned} \quad (6)$$

is the rate by user $j(k)$ in decoding its own message, and

$$\begin{aligned} r_{j(k)}^1(\boldsymbol{\tau}, \mathbf{p}, h, \theta) &= \tau_k \ln \left(1 + \frac{p_{j(k)} \bar{h}_k(h, \theta)}{\sigma_B \tau_k + p_k \bar{h}_k(h, \theta)} \right) \\ &= \tau_k \ln \left(1 + \frac{gp_{j(k)}}{\sigma_B \tau_k \theta (d_k + h) + gp_k} \right), k \in \{1, 2, \dots, K/2\} \end{aligned} \quad (7)$$

is the rate by user k in decoding the user $j(k)$'s message.

The optimization problem is to find the optimal values of bandwidth allocation $\boldsymbol{\tau}$, power allocation \mathbf{p} , UAV altitude \sqrt{h} , and antenna beamwidth $\sqrt{\theta}$, with the objective of maximizing the worst user's rate. It can be formulated mathematically as follows:

$$\max_{\boldsymbol{\tau}, \mathbf{p}, h, \theta} f^{\text{NOMA}}(\boldsymbol{\tau}, \mathbf{p}, h, \theta) \triangleq \min_{k=1, \dots, K} r_k^{\text{NOMA}}(\boldsymbol{\tau}, \mathbf{p}, h, \theta) \quad (8a)$$

$$\text{s.t.} \quad (1),$$

$$h_{\min}^2 \leq h \leq h_{\max}^2, \theta_{\min}^2 \leq \theta \leq \theta_{\max}^2, \quad (8b)$$

$$\sum_{k=1}^{K/2} \tau_k = 1, \quad \& \quad \tau_k \geq 0, \quad \forall k \in \{1, \dots, K/2\} \quad (8c)$$

$$\sum_{k=1}^K p_k = P, \quad (8d)$$

where

$$r_k^{\text{NOMA}}(\boldsymbol{\tau}, \mathbf{p}, h, \theta) = \begin{cases} r_k(\boldsymbol{\tau}, \mathbf{p}, h, \theta), & k \in \{1, \dots, K/2\}, \\ r_{j(k)}(\boldsymbol{\tau}, \mathbf{p}, h, \theta), & j(k) \in \{K/2 + 1, \dots, K\}, \end{cases}$$

$r_k(\boldsymbol{\tau}, \mathbf{p}, h, \theta)$ is given by (4), $r_{j(k)}(\boldsymbol{\tau}, \mathbf{p}, h, \theta)$ is given by (5), P is the total power budget, and θ_{\min} and θ_{\max} specify the allowed range of the antenna beamwidth, i.e., $(0, \pi/2)$. It is quite challenging to solve the non-convex problem (8) because the objective function (8a) is non-convex and non-linear function of four different types of variables, i.e., power, bandwidth, altitude, and beamwidth. In addition, it is also challenging to handle the coverage constraint, which is dependent nonlinearly on the beamwidth and UAV altitude. In Section III, we will provide an inner convex approximation-based path-following algorithm to solve this problem.

B. DPC Problem Formulation

For two users sharing the same bandwidth, the DPC is practical [27]–[29], under which the rate of user $k \in \{1, \dots, K/2\}$ is defined by (4) while the rate of user $j(k) \in \{K/2 + 1, \dots, K\}$ is defined

by (6). Thus, the max-min rate optimization problem under DPC can be formulated as follows:

$$\max_{\boldsymbol{\tau}, \mathbf{p}, h, \theta} f^{\text{DPC}}(\boldsymbol{\tau}, \mathbf{p}, h, \theta) \triangleq \min_{k=1, \dots, K} r_k^{\text{DPC}}(\boldsymbol{\tau}, \mathbf{p}, h, \theta) \quad \text{s.t.} \quad (1), (8b) - (8d), \quad (9)$$

where

$$r_k^{\text{DPC}}(\boldsymbol{\tau}, \mathbf{p}, h, \theta) = \begin{cases} r_k(\boldsymbol{\tau}, \mathbf{p}, h, \theta), & k \in \{1, \dots, K/2\}, \\ r_{j(k)}^2(\boldsymbol{\tau}, \mathbf{p}, h, \theta), & j(k) \in \{K/2 + 1, \dots, K\}, \end{cases}$$

$r_k(\boldsymbol{\tau}, \mathbf{p}, h, \theta)$ is given by (4) and far-user rate $r_{j(k)}^2(\boldsymbol{\tau}, \mathbf{p}, h, \theta)$ is defined in (6).

C. OMA Problem Formulation

For OMA, the optimization problem can be formulated in two ways. The first way, which we term ‘‘OMA-1’’ is to allocate distinct bandwidth to all users, i.e., in (3), $w_k = \tau_k \mathcal{B}$, will be defined for $k \in \{1, \dots, K\}$. Thus, under this OMA-1, the optimization problem can be formulated as follows:

$$\max_{\boldsymbol{\tau}, \mathbf{p}, h, \theta} f^{\text{OMA-1}}(\boldsymbol{\tau}, \mathbf{p}, h, \theta) \triangleq \min_{k=1, \dots, K} r_k^{\text{OMA-1}}(\boldsymbol{\tau}, \mathbf{p}, h, \theta) \quad \text{s.t.} \quad (8b), (8d), \quad (10a)$$

$$\sum_{k=1}^K \tau_k = 1, \quad \& \quad \tau_k \geq 0, \quad \forall k \in \{1, \dots, K\} \quad (10b)$$

where $r_k^{\text{OMA-1}}(\boldsymbol{\tau}, \mathbf{p}, h, \theta) = r_k(\boldsymbol{\tau}, \mathbf{p}, h, \theta)$, $\forall k = \{1, \dots, K\}$ and $r_k(\boldsymbol{\tau}, \mathbf{p}, h, \theta)$ is defined in (4).

The second option, which we term ‘‘OMA-2’’, is to find optimal $K/2$ bandwidth partitions along with optimal altitude, power, and antenna beamwidth, and solve the following optimization problem:

$$\max_{\boldsymbol{\tau}, \mathbf{p}, h, \theta} f^{\text{OMA-2}}(\boldsymbol{\tau}, \mathbf{p}, h, \theta) \triangleq \min_{k=1, \dots, K/2} r_k^{\text{OMA-2}}(\boldsymbol{\tau}, \mathbf{p}, h, \theta) \quad \text{s.t.} \quad (8b) - (8d), \quad (11)$$

where

$$r_k^{\text{OMA-2}}(\boldsymbol{\tau}, \mathbf{p}, h, \theta) = \begin{cases} r_k^{\text{O}}(\boldsymbol{\tau}, \mathbf{p}, h, \theta), & k \in \{1, \dots, K/2\}, \\ r_{j(k)}^{\text{O}}(\boldsymbol{\tau}, \mathbf{p}, h, \theta), & j(k) \in \{K/2 + 1, \dots, K\}, \end{cases}$$

such that

$$\begin{aligned}
r_k^{\text{O}}(\boldsymbol{\tau}, \mathbf{p}, h, \theta) &= \tau_k \ln \left(1 + \frac{p_k \bar{h}_k(h, \theta)}{\sigma_B \tau_k + p_{j(k)} \bar{h}_k(h, \theta)} \right) \\
&= \tau_k \ln \left(1 + \frac{gp_k}{\sigma_B \tau_k \theta (d_k + h) + gp_{j(k)}} \right), \quad k \in \{1, \dots, K/2\}, \\
r_{j(k)}^{\text{O}}(\boldsymbol{\tau}, \mathbf{p}, h, \theta) &= \tau_k \ln \left(1 + \frac{p_{j(k)} \bar{h}_{j(k)}(h, \theta)}{\sigma_B \tau_k + p_k \bar{h}_{j(k)}(h, \theta)} \right) \\
&= \tau_k \ln \left(1 + \frac{gp_{j(k)}}{\sigma_B \tau_k \theta (d_{j(k)} + h) + gp_k} \right), \quad j(k) \in \{K/2, \dots, K\}.
\end{aligned} \tag{12}$$

III. ALGORITHMS

In this section, we will solve the formulated problems in Section II, which are non-convex optimization problems and thus pose computational challenges.

A. NOMA Algorithm

From the definitions (5), (6), and (7), one can see that the objective function (8a) of the optimization problem (8) is a complex non-concave function. Also, constraint (1) is also non-convex. To obtain a path-following computational procedure [30], [31], which improves a feasible point of (8) after each iteration and converges to an optimal solution, we need to develop a lower-bounding concave approximation for the objective function and also an inner convex approximation for constraint (1).

Let $(\boldsymbol{\tau}^{(\kappa)}, \mathbf{p}^{(\kappa)}, h^{(\kappa)}, \theta^{(\kappa)})$ be a feasible point for (8) that is found at the $(\kappa - 1)$ th iteration. With regard to the function r_k in (8), applying inequality (46) in the appendix for

$$\tau = \tau_k, x = \sigma_B \theta / gp_k, y = \tau_k (d_k + h)$$

and

$$\bar{\tau} = \tau_k^{(\kappa)}, \bar{x} = \sigma_B \theta^{(\kappa)} / gp_k^{(\kappa)}, \bar{y} = \tau_k^{(\kappa)} (d_k + h^{(\kappa)})$$

yields

$$r_k(\boldsymbol{\tau}, \mathbf{p}, h, \theta) \geq a_k^{(\kappa)} + b_k^{(\kappa)} \left(2 - \frac{p_k^{(\kappa)} \theta}{\theta^{(\kappa)} p_k} - \frac{\tau_k (d_k + h)}{\tau_k^{(\kappa)} (d_k + h^{(\kappa)})} \right) - \frac{c_k^{(\kappa)}}{\tau_k} \tag{13}$$

where

$$0 < a_k^{(\kappa)} = 2\bar{\tau} \ln(1 + 1/\bar{x}\bar{y}), \quad 0 < b_k^{(\kappa)} = \frac{\bar{\tau}}{1 + \bar{x}\bar{y}}, \quad 0 < c_k^{(\kappa)} = \bar{\tau}^2 \ln(1 + 1/\bar{x}\bar{y}). \quad (14)$$

From (13) it remains to deal with

$$\begin{aligned} \frac{p_k^{(\kappa)} \theta}{\theta^{(\kappa)} p_k} &= \frac{1}{4} \left(\left(\frac{\theta}{\theta^{(\kappa)}} + \frac{p_k^{(\kappa)}}{p_k} \right)^2 - \left(\frac{\theta}{\theta^{(\kappa)}} - \frac{p_k^{(\kappa)}}{p_k} \right)^2 \right) \\ &\leq \frac{1}{4} \left(\frac{\theta}{\theta^{(\kappa)}} + \frac{p_k^{(\kappa)}}{p_k} \right)^2 \\ &\triangleq \pi_k^{(\kappa)}(\theta, p_k) \end{aligned} \quad (15)$$

and

$$\begin{aligned} \frac{\tau_k(d_k + h)}{\tau_k^{(\kappa)}(d_k + h^{(\kappa)})} &= \frac{1}{4} \left(\left(\frac{\tau_k}{\tau_k^{(\kappa)}} + \frac{d_k + h}{d_k + h^{(\kappa)}} \right)^2 - \left(\frac{\tau_k}{\tau_k^{(\kappa)}} - \frac{d_k + h}{d_k + h^{(\kappa)}} \right)^2 \right) \\ &\leq \frac{1}{4} \left(\frac{\tau_k}{\tau_k^{(\kappa)}} + \frac{d_k + h}{d_k + h^{(\kappa)}} \right)^2 \\ &\triangleq \varphi_k^{(\kappa)}(\tau_k, h) \end{aligned} \quad (16)$$

Therefore,

$$r_k(\boldsymbol{\tau}, \mathbf{p}, h, \theta) \geq r_k^{(\kappa)}(\boldsymbol{\tau}, \mathbf{p}, h, \theta) \quad (17)$$

for

$$r_k^{(\kappa)}(\boldsymbol{\tau}, \mathbf{p}, h, \theta) \triangleq a_k^{(\kappa)} + b_k^{(\kappa)} \left(2 - \pi_k^{(\kappa)}(\theta, p_k) - \varphi_k^{(\kappa)}(\tau_k, h) \right) - \frac{c_k^{(\kappa)}}{\tau_k}, \quad (18)$$

which is a concave function. With regard to the function $r_{j(k)}^2$, applying inequality (46) in the appendix for

$$\tau = \tau_k, \quad x = \sigma_B \theta / gp_{j(k)}, \quad y = \tau_k(d_{j(k)} + h) + gp_k / (\sigma_B \theta)$$

and

$$\bar{\tau} = \tau_k^{(\kappa)}, \quad \bar{x} = \sigma_B \theta^{(\kappa)} / gp_{j(k)}^{(\kappa)}, \quad \bar{y} = \tau_k^{(\kappa)}(d_{j(k)} + h^{(\kappa)}) + gp_k^{(\kappa)} / (\theta^{(\kappa)} \sigma_B)$$

yields

$$r_{j(k)}^2(\boldsymbol{\tau}, \mathbf{p}, h, \theta) \geq a_{j(k)}^{(\kappa)} + b_{j(k)}^{(\kappa)} \left(2 - \frac{p_{j(k)}^{(\kappa)}}{\theta^{(\kappa)}} \frac{\theta}{p_{j(k)}} - \frac{\tau_k(d_{j(k)} + h) + gp_k/(\sigma_B\theta)}{\tau_k^{(\kappa)}(d_{j(k)} + h^{(\kappa)}) + gp_k^{(\kappa)}/(\sigma_B\theta^{(\kappa)})} \right) - \frac{c_{j(k)}^{(\kappa)}}{\tau_k} \quad (19)$$

where

$$0 < a_{j(k)}^{(\kappa)} = 2\bar{\tau} \ln(1 + 1/\bar{x}\bar{y}), \quad 0 < b_{j(k)}^{(\kappa)} = \frac{\bar{\tau}}{1 + \bar{x}\bar{y}}, \quad 0 < c_{j(k)}^{(\kappa)} = \bar{\tau}^2 \ln(1 + 1/\bar{x}\bar{y}). \quad (20)$$

From (19), it remains to deal with

$$\begin{aligned} \frac{p_{j(k)}^{(\kappa)}}{\theta^{(\kappa)}} \frac{\theta}{p_{j(k)}} &\leq \frac{1}{4} \left(\frac{p_{j(k)}^{(\kappa)}}{p_{j(k)}} + \frac{\theta}{\theta^{(\kappa)}} \right)^2 \\ &\triangleq \pi_{j(k)}^{(\kappa)}(p_{j(k)}, \theta), \end{aligned} \quad (21)$$

and

$$\begin{aligned} &\frac{\tau_k(d_{j(k)} + h) + gp_k/(\sigma_B\theta)}{\tau_k^{(\kappa)}(d_{j(k)} + h^{(\kappa)}) + gp_k^{(\kappa)}/(\sigma_B\theta^{(\kappa)})} = \\ &\frac{(\tau_k/\tau_k^{(\kappa)}) \cdot [(d_{j(k)} + h)/(d_{j(k)} + h^{(\kappa)})]}{1 + gp_k^{(\kappa)}/\sigma_B\theta^{(\kappa)}\tau_k^{(\kappa)}(d_{j(k)} + h^{(\kappa)})} + \frac{(p_k/p_k^{(\kappa)}) \cdot (\theta^{(\kappa)}/\theta)}{\sigma_B\theta^{(\kappa)}\tau_k^{(\kappa)}(d_{j(k)} + h^{(\kappa)})/gp_k^{(\kappa)} + 1} \leq \\ &\frac{1}{4} \frac{\left((\tau_k/\tau_k^{(\kappa)}) + (d_{j(k)} + h)/(d_{j(k)} + h^{(\kappa)}) \right)^2}{1 + gp_k^{(\kappa)}/\sigma_B\theta^{(\kappa)}\tau_k^{(\kappa)}(d_{j(k)} + h^{(\kappa)})} + \frac{1}{4} \frac{\left((p_k/p_k^{(\kappa)}) + (\theta^{(\kappa)}/\theta) \right)^2}{\sigma_B\theta^{(\kappa)}\tau_k^{(\kappa)}(d_{j(k)} + h^{(\kappa)})/gp_k^{(\kappa)} + 1} \triangleq \\ &\nu_k^{(\kappa)}(\tau_k, p_k, \theta). \end{aligned} \quad (22)$$

Therefore,

$$r_{j(k)}^2(\boldsymbol{\tau}, \mathbf{p}, h, \theta) \geq r_{j(k)}^{2,(\kappa)}(\boldsymbol{\tau}, \mathbf{p}, h, \theta) \quad (23)$$

for

$$r_{j(k)}^{2,(\kappa)}(\boldsymbol{\tau}, \mathbf{p}, h, \theta) \triangleq a_{j(k)}^{(\kappa)} + b_{j(k)}^{(\kappa)} \left(2 - \pi_{j(k)}^{(\kappa)}(\theta, p_{j(k)}) - \nu_k^{(\kappa)}(\tau_k, p_k, \theta) \right) - \frac{c_{j(k)}^{(\kappa)}}{\tau_k}. \quad (24)$$

Analogously,

$$\begin{aligned} r_{j(k)}^1(\boldsymbol{\tau}, \mathbf{p}, h, \theta) &\geq \tilde{a}_{j(k)}^{(\kappa)} + \tilde{b}_{j(k)}^{(\kappa)} \left(2 - \frac{p_{j(k)}^{(\kappa)}}{\theta^{(\kappa)}} \frac{\theta}{p_{j(k)}} - \frac{\tau_k(d_k + h) + gp_k/(\sigma_B\theta)}{\tau_k^{(\kappa)}(d_k + h^{(\kappa)}) + gp_k^{(\kappa)}/(\sigma_B\theta^{(\kappa)})} \right) - \frac{\tilde{c}_{j(k)}^{(\kappa)}}{\tau_k} \\ &\geq r_{j(k)}^{1,(\kappa)}(\boldsymbol{\tau}, \mathbf{p}, h, \theta) \end{aligned} \quad (25)$$

for

$$r_{j(k)}^{1,(\kappa)}(\boldsymbol{\tau}, \mathbf{p}, h, \theta) \triangleq \tilde{a}_{j(k)}^{(\kappa)} + \tilde{b}_{j(k)}^{(\kappa)} \left(2 - \pi_{j(k)}^{(\kappa)}(\theta, p_{j(k)}) - \tilde{\nu}_k^{(\kappa)}(\tau_k, p_k, \theta) \right) - \frac{\tilde{c}_{j(k)}^{(\kappa)}}{\tau_k}, \quad (26)$$

and

$$\tilde{\nu}_k^{(\kappa)}(\tau_k, p_k, \theta) \triangleq \frac{1}{4} \frac{\left((\tau_k/\tau_k^{(\kappa)}) + (d_k + h)/(d_k + h^{(\kappa)}) \right)^2}{1 + gp_k^{(\kappa)}/\sigma_B\theta^{(\kappa)}\tau_k^{(\kappa)}(d_k + h^{(\kappa)})} + \frac{1}{4} \frac{\left((p_k/p_k^{(\kappa)}) + (\theta^{(\kappa)}/\theta) \right)^2}{\sigma_B\theta^{(\kappa)}\tau_k^{(\kappa)}(d_k + h^{(\kappa)})/gp_k^{(\kappa)} + 1}, \quad (27)$$

and

$$\tilde{a}_{j(k)}^{(\kappa)} = 2\bar{\tau} \ln(1 + 1/\bar{x}\bar{y}), \quad \tilde{b}_{j(k)}^{(\kappa)} = \frac{\bar{\tau}}{1 + \bar{x}\bar{y}}, \quad \tilde{c}_{j(k)}^{(\kappa)} = \bar{\tau}^2 \ln(1 + 1/\bar{x}\bar{y}), \quad (28)$$

under

$$\bar{\tau} = \tau_k^{(\kappa)}, \quad \bar{x} = \sigma_B\theta^{(\kappa)}/gp_k^{(\kappa)}, \quad \bar{y} = \tau_k^{(\kappa)}(d_k + h^{(\kappa)}) + gp_k^{(\kappa)}/(\sigma_B\theta^{(\kappa)}).$$

A lower bounding concave function for the objective function (8a) is

$$f^{\text{NOMA},(\kappa)}(\boldsymbol{\tau}, \mathbf{p}, h, \theta) = \min_{k=1, \dots, K} r_k^{\text{NOMA},(\kappa)}(\boldsymbol{\tau}, \mathbf{p}, h, \theta) \quad (29)$$

where

$$r_k^{\text{NOMA},(\kappa)}(\boldsymbol{\tau}, \mathbf{p}, h, \theta) = \begin{cases} r_k^{(\kappa)}(\boldsymbol{\tau}, \mathbf{p}, h, \theta), & k \in \{1, \dots, K/2\}, \\ r_{j(k)}^{(\kappa)}(\boldsymbol{\tau}, \mathbf{p}, h, \theta), & j(k) \in \{K/2 + 1, \dots, K\}, \end{cases} \quad (30)$$

and

$$r_{j(k)}^{(\kappa)}(\boldsymbol{\tau}, \mathbf{p}, h, \theta) = \min \left\{ r_{j(k)}^{1,(\kappa)}(\boldsymbol{\tau}, \mathbf{p}, h, \theta), r_{j(k)}^{2,(\kappa)}(\boldsymbol{\tau}, \mathbf{p}, h, \theta) \right\}.$$

with $r_k^{(\kappa)}(\boldsymbol{\tau}, \mathbf{p}, h, \theta)$, $r_{j(k)}^{1,(\kappa)}(\boldsymbol{\tau}, \mathbf{p}, h, \theta)$, and $r_{j(k)}^{2,(\kappa)}(\boldsymbol{\tau}, \mathbf{p}, h, \theta)$ defined in (18), (26), and (24), respectively.

It remains to deal with the non-convex constraint (1). From the convexity of the tangential function,

it follows that

$$\begin{aligned} \sqrt{h} \tan \sqrt{\theta} &\geq \sqrt{h} \left(\tan \sqrt{\theta^{(\kappa)}} + \frac{\sqrt{\theta} - \sqrt{\theta^{(\kappa)}}}{(\cos \sqrt{\theta^{(\kappa)}})^2} \right) \\ &= \frac{\sin \sqrt{\theta^{(\kappa)}} \cos \sqrt{\theta^{(\kappa)}} - \sqrt{\theta^{(\kappa)}}}{(\cos \sqrt{\theta^{(\kappa)}})^2} \sqrt{h} + \frac{\sqrt{h\theta}}{(\cos \sqrt{\theta^{(\kappa)}})^2} \\ &\geq \frac{\sin \sqrt{\theta^{(\kappa)}} \cos \sqrt{\theta^{(\kappa)}} - \sqrt{\theta^{(\kappa)}}}{(\cos \sqrt{\theta^{(\kappa)}})^2} \left(\frac{\sqrt{h^{(\kappa)}}}{2} + \frac{h}{2\sqrt{h^{(\kappa)}}} \right) + \frac{\sqrt{h\theta}}{(\cos \sqrt{\theta^{(\kappa)}})^2}. \end{aligned} \quad (31)$$

Therefore, an inner approximation of (1) is¹

$$R \leq \frac{\sin \sqrt{\theta^{(\kappa)}} \cos \sqrt{\theta^{(\kappa)}} - \sqrt{\theta^{(\kappa)}}}{(\cos \sqrt{\theta^{(\kappa)}})^2} \left(\frac{\sqrt{h^{(\kappa)}}}{2} + \frac{h}{2\sqrt{h^{(\kappa)}}} \right) + \frac{\sqrt{h\theta}}{(\cos \sqrt{\theta^{(\kappa)}})^2}, \quad (32)$$

i.e. every feasible point for the latter is also feasible for the former.

In summary, at the κ -th iteration, we solve the following convex optimization problem to generate the next iterative feasible point $(\tau^{(\kappa+1)}, \mathbf{p}^{(\kappa+1)}, \theta^{(\kappa+1)}, h^{(\kappa+1)})$:

$$\max_{\tau, \mathbf{p}, h, \theta} f^{\text{NOMA}, (\kappa)}(\tau, \mathbf{p}, h, \theta) \quad \text{s.t.} \quad (8b), (8c), (8d), (32), \quad (33)$$

Algorithm 1 outlines the steps to solve the max-min rate optimization problem (8).

Finding an initial feasible point: The initial feasible point $(\tau^{(0)}, \mathbf{p}^{(0)}, \theta^{(0)}, h^{(0)})$ can be obtained by following the following three steps.

- 1) First, we can calculate $\tau^{(0)}$ and $\mathbf{p}^{(0)}$ by simply assuming equal power and equal bandwidth allocation, i.e., $p_k^{(0)} = P/K, \forall k$, and $\tau_k^{(0)} = 1/(K/2), \forall k \in \{1, \dots, K/2\}$.
- 2) We can find $\theta^{(0)}$ by fixing it to some value that satisfies $\theta_{\min}^2 \leq \theta \leq \theta_{\max}^2$ in (8b).
- 3) Finally, we can find $h^{(0)}$ by solving a feasibility problem for h under convex constraints

$$h_{\min}^2 \leq h \leq h_{\max}^2 \quad \text{and} \quad R \leq \sqrt{h} \tan \sqrt{\theta^{(0)}}.$$

Note that $f^{\text{NOMA}, (\kappa)}(\tau^{(\kappa+1)}, \mathbf{p}^{(\kappa+1)}, h^{(\kappa+1)}, \theta^{(\kappa+1)}) > f^{\text{NOMA}, (\kappa)}(\tau^{(\kappa)}, \mathbf{p}^{(\kappa)}, h^{(\kappa)}, \theta^{(\kappa)})$ because $(\tau^{(\kappa+1)}, \mathbf{p}^{(\kappa+1)}, h^{(\kappa+1)}, \theta^{(\kappa+1)})$ and $(\tau^{(\kappa)}, \mathbf{p}^{(\kappa)}, h^{(\kappa)}, \theta^{(\kappa)})$ are respectively the optimal solution and a feasible point of (33). Therefore

$$f^{\text{NOMA}}(\tau^{(\kappa+1)}, \mathbf{p}^{(\kappa+1)}, h^{(\kappa+1)}, \theta^{(\kappa+1)}) \geq f^{\text{NOMA}, (\kappa)}(\tau^{(\kappa+1)}, \mathbf{p}^{(\kappa+1)}, h^{(\kappa+1)}, \theta^{(\kappa+1)}) \quad (34)$$

$$\begin{aligned} &> f^{\text{NOMA}, (\kappa)}(\tau^{(\kappa)}, \mathbf{p}^{(\kappa)}, h^{(\kappa)}, \theta^{(\kappa)}) \\ &= f^{\text{NOMA}}(\tau^{(\kappa)}, \mathbf{p}^{(\kappa)}, h^{(\kappa)}, \theta^{(\kappa)}), \end{aligned} \quad (35)$$

where (34) is true because $f^{\text{NOMA}, (\kappa)}$ is a lower bound of f^{NOMA} while (35) is true because $f^{\text{NOMA}, (\kappa)}$ matches with f^{NOMA} at $(\tau^{(\kappa)}, \mathbf{p}^{(\kappa)}, h^{(\kappa)}, \theta^{(\kappa)})$, so $(\tau^{(\kappa+1)}, \mathbf{p}^{(\kappa+1)}, h^{(\kappa+1)}, \theta^{(\kappa+1)})$ is a better feasible

¹ $\sin \sqrt{\theta^{(\kappa)}} \cos \sqrt{\theta^{(\kappa)}} - \sqrt{\theta^{(\kappa)}} < 0$

Algorithm 1 NOMA-based algorithm for max-min rate optimization problem (8)

Initialization: Set $\kappa := 0$ and a feasible point $(\boldsymbol{\tau}^{(0)}, \mathbf{p}^{(0)}, \theta^{(0)}, h^{(0)})$ for constraints (1), (8b), (8c), and (8d).

1: **repeat**

2: Solve the convex optimization problem (33) to obtain the optimal solution $(\boldsymbol{\tau}^{(\kappa+1)}, \mathbf{p}^{(\kappa+1)}, \theta^{(\kappa+1)}, h^{(\kappa+1)})$.

3: Set $\kappa := \kappa + 1$.

4: **until** Convergence

point than $(\boldsymbol{\tau}^{(\kappa)}, \mathbf{p}^{(\kappa)}, h^{(\kappa)}, \theta^{(\kappa)})$. As such, the sequence $\{(\boldsymbol{\tau}^{(\kappa)}, \mathbf{p}^{(\kappa)}, h^{(\kappa)}, \theta^{(\kappa)})\}$ at least converges to a locally optimal solution of (8) [30], [31].

B. DPC Algorithm

The objective function of the DPC problem (9) has structure similar to that for the NOMA problem (8). The non-convex constraint (1) can be approximated by (32). Thus, we can use the inequality (46) and approximations (15), (16), (21), and (22), to approximate the non-concave objective function in (9). Therefore, at the κ -th iteration, we solve the following convex optimization problem to generate the next iterative feasible point $(\boldsymbol{\tau}^{(\kappa+1)}, \mathbf{p}^{(\kappa+1)}, \theta^{(\kappa+1)}, h^{(\kappa+1)})$:

$$\max_{\boldsymbol{\tau}, \mathbf{p}, h, \theta} f^{\text{DPC}, (\kappa)} \triangleq \min_{k=1, \dots, K/2} r_k^{\text{DPC}, (\kappa)}(\boldsymbol{\tau}, \mathbf{p}, h, \theta) \quad \text{s.t.} \quad (8b), (8c), (8d), (32), \quad (36)$$

where

$$r_k^{\text{DPC}, (\kappa)}(\boldsymbol{\tau}, \mathbf{p}, h, \theta) = \begin{cases} r_k^{(\kappa)}(\boldsymbol{\tau}, \mathbf{p}, h, \theta), & k \in \{1, \dots, K/2\}, \\ r_{j(k)}^{2, (\kappa)}(\boldsymbol{\tau}, \mathbf{p}, h, \theta), & j(k) \in \{K/2 + 1, \dots, K\}. \end{cases}$$

Note that $r_k^{(\kappa)}(\boldsymbol{\tau}, \mathbf{p}, h, \theta)$ and $r_{j(k)}^{2, (\kappa)}(\boldsymbol{\tau}, \mathbf{p}, h, \theta)$ are defined in (18) and (24), respectively.

Algorithm 2 DPC-based algorithm for max-min rate optimization problem (9)

Initialization: Set $\kappa := 0$ and a feasible point $(\boldsymbol{\tau}^{(0)}, \mathbf{p}^{(0)}, \theta^{(0)}, h^{(0)})$ for constraints (1), (8b), (8c), and (8d).

1: **repeat**

2: Solve the convex optimization problem (36) to obtain the optimal solution $(\boldsymbol{\tau}^{(\kappa+1)}, \mathbf{p}^{(\kappa+1)}, \theta^{(\kappa+1)}, h^{(\kappa+1)})$.

3: Set $\kappa := \kappa + 1$.

4: **until** Convergence

Similar to Algorithm 1, Algorithm 2 outlines the steps to solve the max-min rate optimization problem (9). The initial feasible point $(\boldsymbol{\tau}^{(0)}, \mathbf{p}^{(0)}, \theta^{(0)}, h^{(0)})$ can be obtained in the same way as described for the NOMA in Section III-A.

C. OMA Algorithm

The objective function of the OMA-1 problem (10) also has similarity in its structure to that for the NOMA problem (8). The non-convex constraint (1) can be approximated by (32). Thus, we can use the inequality (46) and the approximations (15) and (16) to approximate the non-concave objective function in (10). Thus, we solve the following convex optimization problem, at the κ -th iteration, to generate the next iterative feasible point $(\boldsymbol{\tau}^{(\kappa+1)}, \mathbf{p}^{(\kappa+1)}, \theta^{(\kappa+1)}, h^{(\kappa+1)})$:

$$\max_{\boldsymbol{\tau}, \mathbf{p}, h, \theta} f^{\text{OMA-1}, (\kappa)} \triangleq \min_{k=1, \dots, K} r_k^{\text{OMA-1}, (\kappa)}(\boldsymbol{\tau}, \mathbf{p}, h, \theta) \quad \text{s.t.} \quad (8b), (10b), (8d), (32), \quad (37)$$

where $r_k^{\text{OMA-1}, (\kappa)}(\boldsymbol{\tau}, \mathbf{p}, h, \theta) = r_k^{(\kappa)}(\boldsymbol{\tau}, \mathbf{p}, h, \theta)$, $\forall k = \{1, \dots, K\}$ and $r_k^{(\kappa)}(\boldsymbol{\tau}, \mathbf{p}, h, \theta)$ is defined in (18). Algorithm 3 outlines the steps to solve the max-min rate optimization problem (10). The initial feasible point $(\boldsymbol{\tau}^{(0)}, \mathbf{p}^{(0)}, \theta^{(0)}, h^{(0)})$ can be obtained in the same way as described for the NOMA in Section III-A.

Algorithm 3 OMA-1 algorithm for max-min rate optimization problem (10)

Initialization: Set $\kappa := 0$ and a feasible point $(\boldsymbol{\tau}^{(0)}, \mathbf{p}^{(0)}, \theta^{(0)}, h^{(0)})$ for constraints (1), (8b), (10b), and (8d).

1: **repeat**

2: Solve the convex optimization problem (37) to obtain the optimal solution $(\boldsymbol{\tau}^{(\kappa+1)}, \mathbf{p}^{(\kappa+1)}, \theta^{(\kappa+1)}, h^{(\kappa+1)})$.

3: Set $\kappa := \kappa + 1$.

4: **until** Convergence

Next, in order to solve the OMA-2 problem (11), at the κ -th iteration, we solve the following convex optimization problem to generate the next iterative feasible point $(\boldsymbol{\tau}^{(\kappa+1)}, \mathbf{p}^{(\kappa+1)}, \theta^{(\kappa+1)}, h^{(\kappa+1)})$:

$$\max_{\boldsymbol{\tau}, \mathbf{p}, h, \theta} f^{\text{OMA-2}, (\kappa)} \quad \min_{k=1, \dots, K/2} r_k^{\text{OMA-2}, (\kappa)}(\boldsymbol{\tau}, \mathbf{p}, h, \theta) \quad \text{s.t.} \quad (8b), (8c), (8d), (32), \quad (38)$$

where

$$r_k^{\text{OMA-2}, (\kappa)}(\boldsymbol{\tau}, \mathbf{p}, h, \theta) = \begin{cases} r_k^{\text{O}, (\kappa)}(\boldsymbol{\tau}, \mathbf{p}, h, \theta), & k \in \{1, \dots, K/2\}, \\ r_{j(k)}^{\text{O}, (\kappa)}(\boldsymbol{\tau}, \mathbf{p}, h, \theta), & j(k) \in \{K/2 + 1, \dots, K\}, \end{cases}$$

where $r_k^{\text{O}, (\kappa)}(\boldsymbol{\tau}, \mathbf{p}, h, \theta)$ and $r_{j(k)}^{\text{O}, (\kappa)}(\boldsymbol{\tau}, \mathbf{p}, h, \theta)$ are inner approximations (at the κ -th iteration) of the non-concave functions $r_k^{\text{O}}(\boldsymbol{\tau}, \mathbf{p}, h, \theta)$ and $r_{j(k)}^{\text{O}}(\boldsymbol{\tau}, \mathbf{p}, h, \theta)$, respectively (defined in (12)). Since $r_{j(k)}^{\text{O}}(\boldsymbol{\tau}, \mathbf{p}, h, \theta)$ is similar to the rate function $r_{j(k)}^2(\boldsymbol{\tau}, \mathbf{p}, h, \theta)$ (defined in (6) for the NOMA-problem) and $r_k^{\text{O}}(\boldsymbol{\tau}, \mathbf{p}, h, \theta)$ has similar structure too, we can use the inequality (46) (given in the appendix) and the approximations (21) and (22) to find the inner approximations $r_k^{\text{O}, (\kappa)}(\boldsymbol{\tau}, \mathbf{p}, h, \theta)$ and $r_{j(k)}^{\text{O}, (\kappa)}(\boldsymbol{\tau}, \mathbf{p}, h, \theta)$.

Thus, by applying the inequality (46) for

$$\tau = \tau_k, x = \sigma_B \theta / gp_k, y = \tau_k(d_k + h) + gp_{j(k)} / (\sigma_B \theta),$$

we can obtain the inner approximation for the non-concave rate function $r_k^{\text{O}}(\boldsymbol{\tau}, \mathbf{p}, h, \theta)$, as follows:

$$r_k^{\text{O}, (\kappa)}(\boldsymbol{\tau}, \mathbf{p}, h, \theta) \triangleq \tilde{a}_k^{\text{O}, (\kappa)} + \tilde{b}_k^{\text{O}, (\kappa)} \left(2 - \pi_k^{(\kappa)}(\theta, p_k) - \tilde{\nu}_{j(k)}^{\text{O}, (\kappa)}(\tau_k, p_{j(k)}, \theta) \right) - \frac{\tilde{c}_k^{\text{O}, (\kappa)}}{\tau_k}, \quad (39)$$

where

$$\tilde{v}_{j(k)}^{O,(\kappa)}(\tau_k, p_{j(k)}, \theta) \triangleq \frac{1}{4} \frac{\left((\tau_k/\tau_k^{(\kappa)}) + (d_k + h)/(d_k + h^{(\kappa)}) \right)^2}{1 + gp_{j(k)}^{(\kappa)}/\sigma_B\theta^{(\kappa)}\tau_k^{(\kappa)}(d_k + h^{(\kappa)})} + \frac{1}{4} \frac{\left((p_{j(k)}/p_{j(k)}^{(\kappa)}) + (\theta^{(\kappa)}/\theta) \right)^2}{\sigma_B\theta^{(\kappa)}\tau_k^{(\kappa)}(d_k + h^{(\kappa)})/gp_{j(k)}^{(\kappa)} + 1}, \quad (40)$$

and

$$\tilde{a}_k^{O,(\kappa)} = 2\bar{\tau} \ln(1 + 1/\bar{x}\bar{y}), \quad \tilde{b}_k^{O,(\kappa)} = \frac{\bar{\tau}}{1 + \bar{x}\bar{y}}, \quad \tilde{c}_k^{O,(\kappa)} = \bar{\tau}^2 \ln(1 + 1/\bar{x}\bar{y}), \quad (41)$$

under

$$\bar{\tau} = \tau_k^{(\kappa)}, \quad \bar{x} = \sigma_B\theta^{(\kappa)}/gp_k^{(\kappa)}, \quad \bar{y} = \tau_k^{(\kappa)}(d_k + h^{(\kappa)}) + gp_{j(k)}^{(\kappa)}/(\sigma_B\theta^{(\kappa)}).$$

Similarly, by applying the inequality (46) for

$$\tau = \tau_k, \quad x = \sigma_B\theta/gp_{j(k)}, \quad y = \tau_k(d_{j(k)} + h) + gp_k/(\sigma_B\theta)$$

we can obtain the inner approximation for the non-concave rate function $r_{j(k)}^O(\boldsymbol{\tau}, \mathbf{p}, h, \theta)$ as follows:

$$r_{j(k)}^{O,(\kappa)}(\boldsymbol{\tau}, \mathbf{p}, h, \theta) \triangleq \tilde{a}_{j(k)}^{O,(\kappa)} + \tilde{b}_{j(k)}^{O,(\kappa)} \left(2 - \pi_{j(k)}^{(\kappa)}(\theta, p_{j(k)}) - \tilde{v}_k^{O,(\kappa)}(\tau_k, p_k, \theta) \right) - \frac{\tilde{c}_{j(k)}^{O,(\kappa)}}{\tau_k}, \quad (42)$$

where

$$\tilde{v}_k^{O,(\kappa)}(\tau_k, p_k, \theta) \triangleq \frac{1}{4} \frac{\left((\tau_k/\tau_k^{(\kappa)}) + (d_{j(k)} + h)/(d_{j(k)} + h^{(\kappa)}) \right)^2}{1 + gp_k^{(\kappa)}/\sigma_B\theta^{(\kappa)}\tau_k^{(\kappa)}(d_{j(k)} + h^{(\kappa)})} + \frac{1}{4} \frac{\left((p_k/p_k^{(\kappa)}) + (\theta^{(\kappa)}/\theta) \right)^2}{\sigma_B\theta^{(\kappa)}\tau_k^{(\kappa)}(d_{j(k)} + h^{(\kappa)})/gp_k^{(\kappa)} + 1}, \quad (43)$$

and

$$\tilde{a}_{j(k)}^{O,(\kappa)} = 2\bar{\tau} \ln(1 + 1/\bar{x}\bar{y}), \quad \tilde{b}_{j(k)}^{O,(\kappa)} = \frac{\bar{\tau}}{1 + \bar{x}\bar{y}}, \quad \tilde{c}_{j(k)}^{O,(\kappa)} = \bar{\tau}^2 \ln(1 + 1/\bar{x}\bar{y}), \quad (44)$$

under

$$\bar{\tau} = \tau_k^{(\kappa)}, \quad \bar{x} = \sigma_B\theta^{(\kappa)}/gp_{j(k)}^{(\kappa)}, \quad \bar{y} = \tau_k^{(\kappa)}(d_{j(k)} + h^{(\kappa)}) + gp_k^{(\kappa)}/(\sigma_B\theta^{(\kappa)}).$$

Algorithm 4 outlines the steps to solve the max-min rate optimization problem (11). The initial feasible point $(\boldsymbol{\tau}^{(0)}, \mathbf{p}^{(0)}, \theta^{(0)}, h^{(0)})$ can be obtained in the same way as described for the NOMA in Section III-A.

Algorithm 4 OMA-2 algorithm for max-min rate optimization problem (11)

Initialization: Set $\kappa := 0$ and a feasible point $(\boldsymbol{\tau}^{(0)}, \mathbf{p}^{(0)}, \theta^{(0)}, h^{(0)})$ for constraints (1), (8b), (8c), and (8d).

1: **repeat**

2: Solve the convex optimization problem (38) to obtain the optimal solution $(\boldsymbol{\tau}^{(\kappa+1)}, \mathbf{p}^{(\kappa+1)}, \theta^{(\kappa+1)}, h^{(\kappa+1)})$.

3: Set $\kappa := \kappa + 1$.

4: **until** Convergence

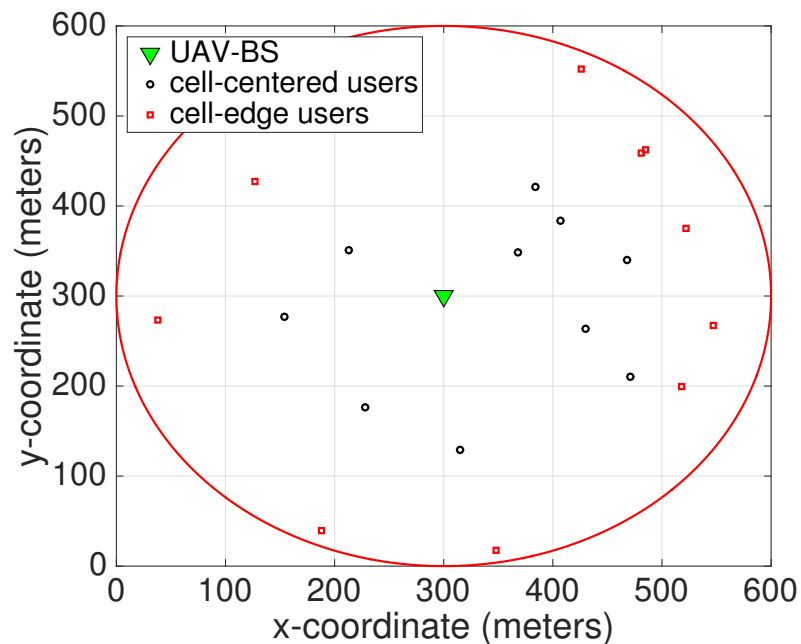


Fig. 2. Network topology used in the simulations.

IV. SIMULATION RESULTS

In this section, we analyze the performance of the proposed Algorithms 1-4 via simulations. We use the network topology as used in Fig. 2, where the cell radius is set to $R = 300$ meters, and there are $K = 20$ users randomly placed within the cell. The UAV BS is at the cell-center and at altitude \sqrt{h} above the ground-level. Fig. 2 shows the ground-level projection of the UAV BS. Half of the

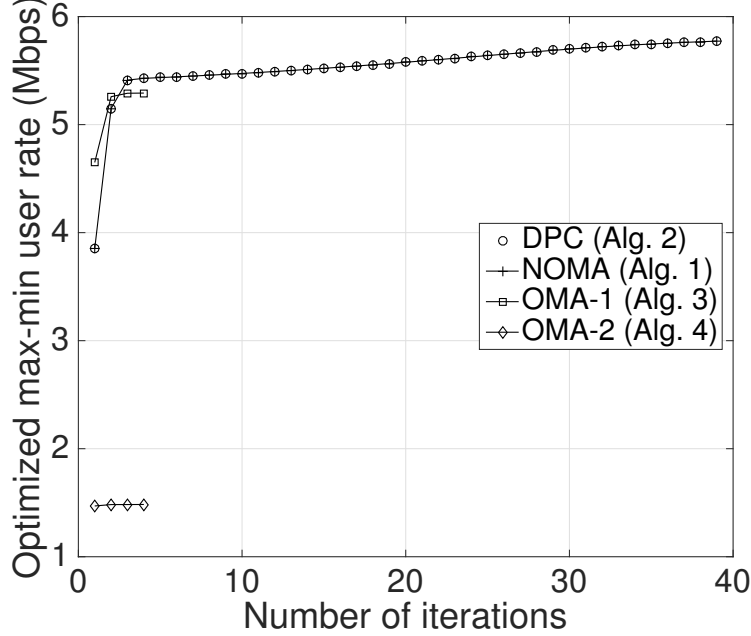


Fig. 3. The convergence of the proposed Algorithms 1-4.

users are placed closer to the UAV BS, while the rest of the users are farther from the UAV BS. The channel power gain at a distance of 1 meter is set to 3.24×10^{-4} , which incorporates -38.47 dB (1.42×10^{-4}) path loss and antenna gain 2.2846 [26]. The maximum and minimum UAV altitude are set to $h_{\max} = 500$ meters and $h_{\min} = 50$ meters, respectively. The range of the antenna beamwidth is set to $\theta_{\min} = 0$ and $\theta_{\max} = \pi/2$ rad. The total power budget is $P = 2$ mW (3 dBm). Unless stated otherwise, we set total available bandwidth $\mathcal{B} = 15$ MHz, and the noise power density $\sigma^2 = -174$ dBm/Hz.

A. Performance of the Proposed Algorithms 1-4

Fig. 3 plots the convergence results of the proposed Algorithms 1-4 employing NOMA problem (8), DPC problem (9), OMA-1 problem (10), and OMA-2 problem (11), respectively. Fig. 3 shows that NOMA (Alg. 1) and DPC (Alg. 2) take around 40 iterations to converge. On the other hand, the convergence of the OMA-1 and OMA-2 (Algorithms 3 and 4) requires only four iterations. However,

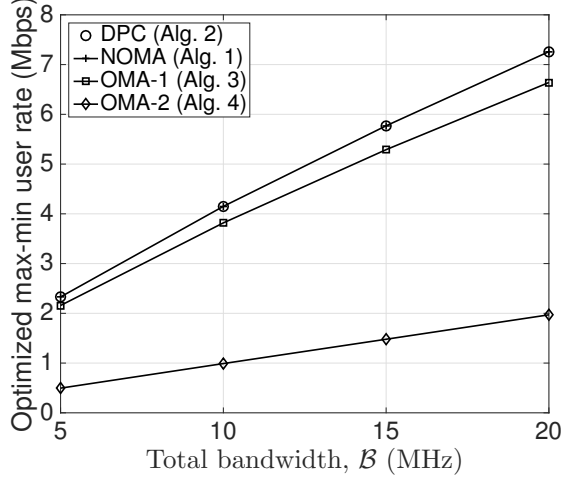


Fig. 4. Optimized max-min user rate versus total available bandwidth B , where the noise power density is set to $\sigma^2 = -174$ dBm/Hz.

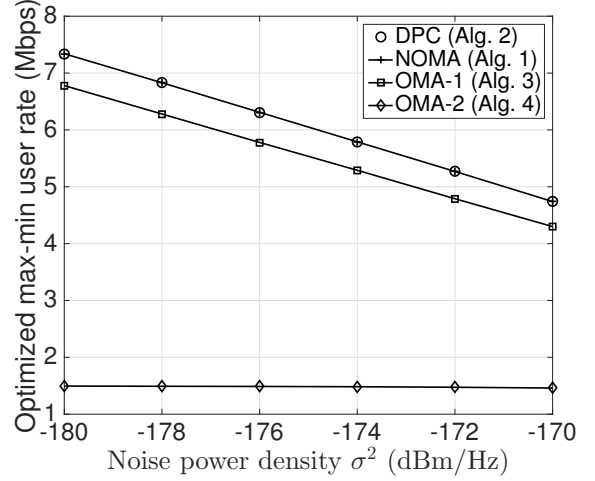


Fig. 5. Optimized max-min user rate versus noise power density σ^2 , where the available bandwidth is set to $B = 15$ MHz.

the NOMA and DPC achieve better rates than their OMA counterparts. Even, at the fourth iteration, which is the point where the OMA-1 (Alg. 3) converges, the optimized rate of the NOMA and DPC is better than that of the OMA-1.

Fig. 4 plots the optimized max-min user rate versus the total available bandwidth B . We solve NOMA problem (8), DPC problem (9), OMA-1 problem (10), and OMA-2 problem (11) using Algorithms 1, 2, 3, and 4, respectively. As expected, the optimized rate increases with an increase in the total available bandwidth B . Fig. 4 shows that the NOMA and DPC achieve the same performance while clearly outperforming the OMA counterparts. Moreover, we observe that the performance gap between the NOMA and OMA-1 increases with an increase in the available bandwidth B .

Fig. 5 plots the optimized max-min user rates of the proposed Algorithms 1-4 versus the noise power density σ^2 . As expected, the optimized rate decreases with an increase in the noise power density σ^2 . Fig. 5 again shows the same trend that the NOMA and DPC clearly outperform the OMA counterparts. In addition, the performance gap between the NOMA and OMA-1 decreases as the noise power density σ^2 increases.

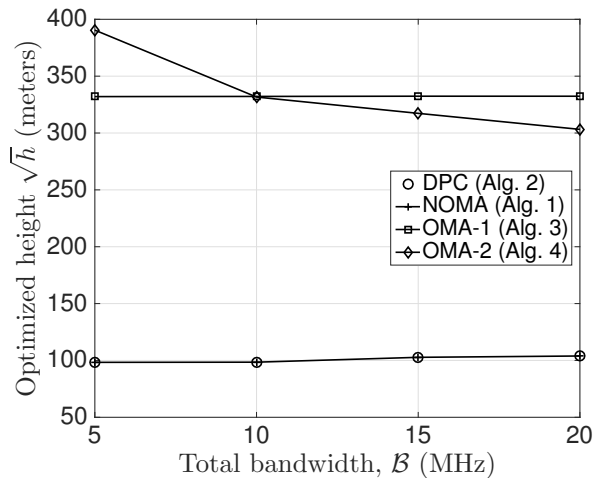


Fig. 6. Optimized altitude \sqrt{h} versus total available bandwidth \mathcal{B} , where the noise power density is set to $\sigma^2 = -174$ dBm/Hz.

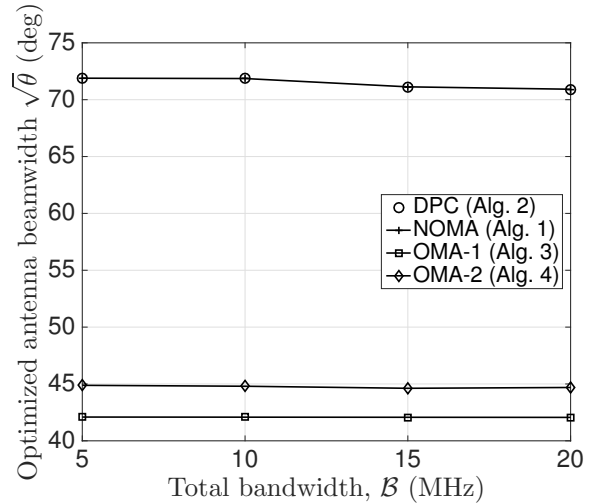


Fig. 7. Optimized antenna beamwidth $\sqrt{\theta}$ versus total available bandwidth \mathcal{B} , where the noise power density is set to $\sigma^2 = -174$ dBm/Hz.

Figs. 6 and 7 plot the optimized values of UAV altitude and antenna beamwidth, respectively, after solving all the problems using Algorithms 1, 2, 3, and 4. Figs. 6 and 7 show that there is minor change in the optimized values of the UAV altitude and antenna beamwidth for different values of the total available bandwidth \mathcal{B} . This is an interesting and desirable result since the UAV is not required to move much if the bandwidth quota changes.

B. Comparison with the Sub-optimal Schemes

Fig. 8 plots the optimized max-min user rate under fixed altitude \sqrt{h} and fixed antenna beamwidth $\sqrt{\theta}$, such that the constraint (1) is satisfied. Again, the bandwidth is set to $\mathcal{B} = 15$ MHz. The Fig. 8(a) assumes $\sqrt{h} = 100$ m, Fig. 8(b) assumes $\sqrt{h} = 200$ m, and Fig. 8(c) assumes $\sqrt{h} = 300$ m. That is, in Fig. 8, we solve the NOMA problem (8), the DPC problem (9), the OMA-1 problem (10), and the OMA-2 problem (11), for given fixed altitude \sqrt{h} and fixed antenna beamwidth $\sqrt{\theta}$, i.e., in the absence of constraint (1). Thus, this sub-optimal scheme requires solving only for the optimal power \mathbf{p} and optimal bandwidth allocation $\boldsymbol{\tau}$. The optimized max-min rates are obviously smaller

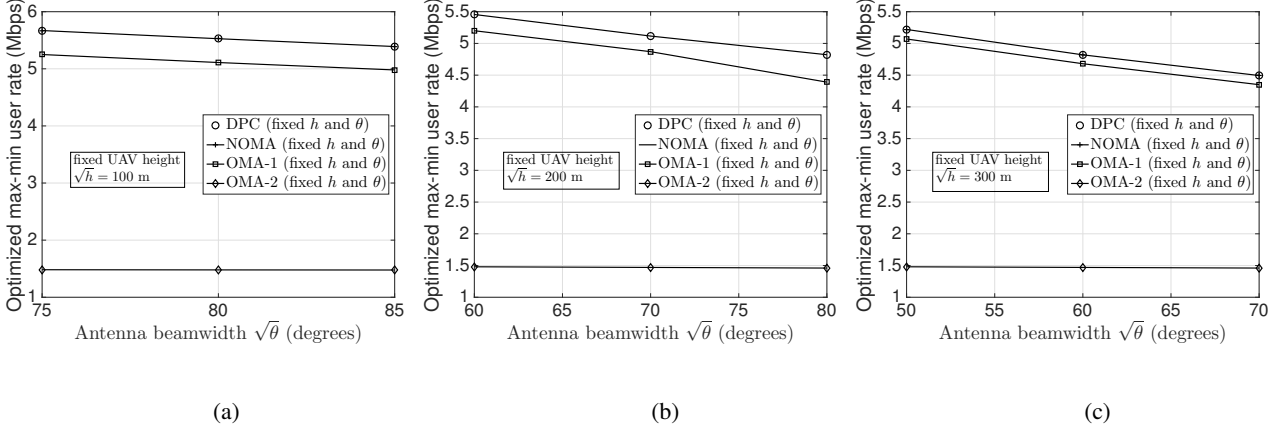


Fig. 8. Optimized max-min user rate under fixed altitude \sqrt{h} and fixed antenna beamwidth $\sqrt{\theta}$, which satisfy (1). Subfig. (a) assumes $\sqrt{h} = 100$ m, subfig. (b) assumes $\sqrt{h} = 200$ m, and subfig. (c) assumes $\sqrt{h} = 300$ m. The total available bandwidth is set to $B = 15$ MHz. If all parameters including UAV altitude and antenna beamwidth are optimized, as in the proposed algorithm, Fig. 4 shows that the optimal rate achieved by NOMA and DPC is 5.77 Mbps, by OMA-1 is 5.29 Mbps, and by OMA-2 is 1.48 Mbps.

than the optimized rates as obtained by the proposed optimal Algorithms 1-4 in Fig. 4. This is because Algorithms 1-4 jointly optimize all the parameters. In addition, *this justifies the desirability of optimizing UAV-BS altitude and antenna beamwidth*. If all parameters including the UAV altitude and antenna beamwidth are optimized, as in the proposed Algorithms 1-4, Fig. 4 shows that the optimal rate achieved by NOMA and DPC is 5.77 Mbps, by OMA-1 is 5.29 Mbps, and by OMA-2 is 1.48 Mbps.

Fig. 9 plots the max-min user rate obtained by another sub-optimal scheme, which assumes fixed power \mathbf{p} and fixed bandwidth τ allocation and solves to find the optimal UAV altitude \sqrt{h} and optimal antenna beamwidth $\sqrt{\theta}$. Fig. 9 plots results for only NOMA (Alg. 1) and OMA-1 (Alg. 3) because DPC provides similar rate as that obtained by NOMA, and the OMA-2 performs quite poorly. Particularly, we opt for equal power and equal bandwidth allocation, such that, equal power allocation implies $p_k = P/K, \forall k$, while equal bandwidth for NOMA means $\tau_k = 1/(K/2), \forall k \in \{1, \dots, K/2\}$ and equal bandwidth allocation for OMA-1 means $\tau_k = 1/K, \forall k \in \{1, \dots, K\}$. Fig. 9 shows that optimal schemes (Algorithms 1 and 3 plotted with solid lines) clearly outperform the

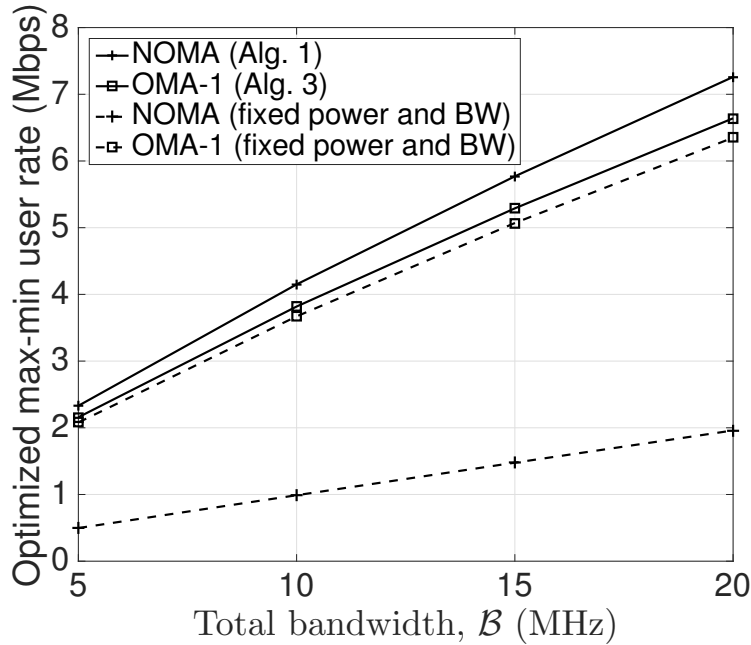


Fig. 9. Comparison of the optimized max-min user rate obtained under fixed power \mathbf{p} and fixed bandwidth τ allocation (equal power and equal bandwidth allocation) with the optimized max-min rate achieved by the proposed algorithms.

respective sub-optimal schemes (plotted with dashed lines). Fig. 9 shows that sub-optimal NOMA performs quite poorly, and even delivers a worse rate than sub-optimal OMA-1. This is because wise power allocation is necessary for NOMA. On the other hand, the sub-optimal NOMA in Fig. 9 assumes equal power allocation, which worsens its achievable rate.

V. CONCLUSIONS

In this paper, we have considered a UAV-enabled communication network which serves a large number of users by employing NOMA. We have formulated the max-min rate optimization problem under total power, total bandwidth, UAV altitude, and antenna beamwidth constraints. The formulated max-min rate objective function is non-convex in the optimization variables, i.e., the UAV's flying altitude, transmit antenna beamwidth, power allocation and bandwidth allocation for multiple users. We have developed a path-following algorithm to solve the formulated problem. In addition, we have also formulated OMA and DPC-based max-min rate optimization problems and developed respective

path-following algorithms to solve them. Finally, our numerical results show that NOMA outperforms OMA and achieves rates similar to those achieved by DPC. Moreover, we have observed a clear rate gain by jointly optimizing all the parameters (power, bandwidth, UAV altitude, and antennas beamwidth), when compared to the case of optimizing subset of these parameters, which confirms the desirability of their joint optimization.

APPENDIX: FUNDAMENTAL INEQUALITIES

For the convex function $f(x, y, t) \triangleq \ln(1 + 1/xy)^{1/t}$ [32], one has the following inequality for every $x > 0, y > 0, t > 0, \bar{x} > 0, \bar{y} > 0$ and $\bar{t} > 0$:

$$\begin{aligned} \frac{\ln(1 + 1/xy)}{t} &= f(x, y, t) \\ &\geq f(\bar{x}, \bar{y}, \bar{t}) + \langle \nabla f(\bar{x}, \bar{y}, \bar{t}), (x, y, t) - (\bar{x}, \bar{y}, \bar{t}) \rangle \\ &= \frac{2 \ln(1 + 1/\bar{x}\bar{y})}{\bar{t}} + \frac{1}{\bar{t}(1 + \bar{x}\bar{y})} (2 - x/\bar{x} - y/\bar{y}) - \frac{\ln(1 + 1/\bar{x}\bar{y})}{\bar{t}^2} t \end{aligned} \quad (45)$$

Therefore, by setting $\tau = 1/t$ and $\bar{\tau} = 1/\bar{t}$,

$$\tau \ln(1 + 1/xy) \geq 2\bar{\tau} \ln(1 + 1/\bar{x}\bar{y}) + \frac{\bar{\tau}}{1 + \bar{x}\bar{y}} (2 - x/\bar{x} - y/\bar{y}) - \frac{\bar{\tau}^2 \ln(1 + 1/\bar{x}\bar{y})}{\tau} \quad (46)$$

REFERENCES

- [1] Y. Zeng, R. Zhang, and T. J. Lim, "Throughput maximization for UAV-enabled mobile relaying systems," *IEEE Trans. Commun.*, vol. 64, no. 12, pp. 4983–4996, Dec. 2016.
- [2] F. Jiang and A. L. Swindlehurst, "Optimization of UAV heading for the ground-to-air uplink," *J. Sel. Areas Commun.*, vol. 30, no. 5, pp. 993–1005, June 2012.
- [3] I. Bor-Yaliniz and H. Yanikomeroglu, "The new frontier in ran heterogeneity: Multi-tier drone-cells," *IEEE Commun. Mag.*, vol. 54, no. 11, pp. 48–55, Nov. 2016.
- [4] H. Menouar, I. Guvenc, K. Akkaya, A. S. Uluogac, A. Kadri, and A. Tuncer, "UAV-enabled intelligent transportation systems for the smart city: Applications and challenges," *IEEE Commun. Mag.*, vol. 55, no. 3, pp. 22–28, Mar. 2017.
- [5] M. Mozaffari, W. Saad, M. Bennis, and M. Debbah, "Mobile unmanned aerial vehicles (UAVs) for energy-efficient internet of things communications," *IEEE Trans. Wirel. Commun.*, vol. 16, no. 11, pp. 7574–7589, Nov. 2017.

- [6] GSMA. Mobile-enabled unmanned aircraft. [Online]. Available: <https://www.gsma.com/iot/mobile-enabled-unmanned-aircraft/>
- [7] P. Zhan, K. Yu, and A. L. Swindlehurst, "Wireless relay communications with unmanned aerial vehicles: Performance and optimization," *IEEE Trans. Aerosp. Electron. Syst.*, vol. 47, no. 3, pp. 2068–2085, 2011.
- [8] M. Erdelj, E. Natalizio, K. R. Chowdhury, and I. F. Akyildiz, "Help from the sky: Leveraging UAVs for disaster management," *IEEE Pervasive Comput.*, vol. 16, no. 1, pp. 24–32, Jan. 2017.
- [9] F. Ono, H. Ochiai, and R. Miura, "A wireless relay network based on unmanned aircraft system with rate optimization," *IEEE Trans. Wirel. Commun.*, vol. 15, no. 11, pp. 7699–7708, Nov. 2016.
- [10] A. Merwaday, A. Tuncer, A. Kumbhar, and I. Guvenc, "Improved throughput coverage in natural disasters: Unmanned aerial base stations for public-safety communications," *IEEE Veh. Technol. Mag.*, vol. 11, no. 4, pp. 53–60, Dec. 2016.
- [11] Y. Zeng, R. Zhang, and T. J. Lim, "Wireless communications with unmanned aerial vehicles: opportunities and challenges," *IEEE Commun. Mag.*, vol. 54, no. 5, pp. 36–42, May 2016.
- [12] Y. Zeng and R. Zhang, "Energy-efficient UAV communication with trajectory optimization," *IEEE Trans. Wirel. Commun.*, vol. 16, no. 6, pp. 3747–3760, Jun. 2017.
- [13] V. V. Chetlur and H. S. Dhillon, "Downlink coverage analysis for a finite 3-D wireless network of unmanned aerial vehicles," *IEEE Trans. Commun.*, vol. 65, no. 10, pp. 4543–4558, Oct. 2017.
- [14] Y. Zeng, X. Xu, and R. Zhang, "Trajectory design for completion time minimization in uav-enabled multicasting," *IEEE Trans. Wirel. Commun.*, vol. 17, no. 4, pp. 2233–2246, Apr. 2018.
- [15] J. Lyu, Y. Zeng, and R. Zhang, "UAV-Aided offloading for cellular hotspot," *IEEE Trans. Wirel. Commun.*, 2018 (Early Access).
- [16] H. He, S. Zhang, Y. Zeng, and R. Zhang, "Joint altitude and beamwidth optimization for UAV-enabled multiuser communications," *IEEE Commun. Lett.*, vol. 22, no. 2, pp. 344–347, 2018.
- [17] H. Ghazzai, M. B. Ghorbel, A. Kadri, M. J. Hossain, and H. Menouar, "Energy-efficient management of unmanned aerial vehicles for underlay cognitive radio systems," *IEEE Trans. Green Commun. Netw.*, vol. 1, no. 4, pp. 434–443, Dec. 2017.
- [18] H. Wang, J. Wang, G. Ding, L. Wang, T. A. Tsiftsis, and P. K. Sharma, "Resource allocation for energy harvesting-powered D2D communication underlying UAV-assisted networks," *IEEE Trans. Green Commun. Netw.*, vol. 2, no. 1, pp. 14–24, Mar. 2018.
- [19] Y. Saito, Y. Kishiyama, A. Benjebbour, T. Nakamura, A. Li, and K. Higuchi, "Non-orthogonal multiple access (NOMA) for cellular future radio access," in *Proc. IEEE Veh. Technol. Conf. (VTC Spring)*, June 2013, pp. 1–5.
- [20] Z. Ding et al., "Application of non-orthogonal multiple access in LTE and 5G networks," *IEEE Commun. Mag.*, vol. 55, no. 2, pp. 185–191, Feb. 2017.
- [21] Z. Ding, F. Adachi, and H. V. Poor, "The application of MIMO to non-orthogonal multiple access," *IEEE Trans. Wireless Commun.*, vol. 15, no. 1, pp. 537–552, Jan. 2016.

- [22] V. D. Nguyen, H. D. Tuan, T. Q. Duong, H. V. Poor, and O. S. Shin, "Precoder design for signal superposition in MIMO-NOMA multicell networks," *IEEE J. Sel. Areas Commun.*, vol. 35, no. 12, pp. 2681–2695, Dec. 2017.
- [23] P. K. Sharma and D. I. Kim, "UAV-enabled downlink wireless system with non-orthogonal multiple access," in *Proc. IEEE Global Commun. Conf.*, Dec. 2017, pp. 1–6.
- [24] N. Rupasinghe, Y. Yapici, I. Guvenc, and Y. Kakishima, "Non-orthogonal multiple access for mmwave drones with multi-antenna transmission," <https://arxiv.org/pdf/1711.10050.pdf>, 2018.
- [25] M. F. Sohail, C. Y. Leow, and S. H. Won, "Non-orthogonal multiple access for unmanned aerial vehicle assisted communication," *IEEE Access*, vol. 6, pp. 22 716 – 22 727, Apr. 2018.
- [26] H. He, S. Zhang, Y. Zeng, and R. Zhang, "Joint altitude and beamwidth optimization for UAV-enabled multiuser communications," *IEEE Commun. Lett.*, vol. 22, no. 2, pp. 344–347, Feb 2018.
- [27] W. Yu and J. M. Cioffi, "Trellis precoding for the broadcast channel," in *Proc. IEEE Global Commun. Conf.*, Nov. 2001, pp. 1344–1383.
- [28] U. Erez and S. ten Brink, "A close-to-capacity dirty paper coding scheme," *IEEE Trans. Inf. Theory*, vol. 51, no. 10, pp. 3417–3432, Oct. 2005.
- [29] U. Erez, S. Shamai, and R. Zamir, "Capacity and lattice strategies for canceling known interference," *IEEE Trans. Inf. Theory*, vol. 51, no. 11, pp. 3820–3833, Nov. 2005.
- [30] H. H. M. Tam, H. D. Tuan, and D. T. Ngo, "Successive convex quadratic programming for quality-of-service management in full-duplex MU-MIMO multicell networks," *IEEE Trans. Commun.*, vol. 64, no. 6, pp. 2340–2353, Jun. 2016.
- [31] H. H. M. Tam, H. D. Tuan, D. T. Ngo, T. Q. Duong, and H. V. Poor, "Joint load balancing and interference management for small-cell heterogeneous networks with limited backhaul capacity," *IEEE Trans. Wirel. Commun.*, vol. 16, no. 2, pp. 872–884, Feb. 2017.
- [32] Z. Sheng, H. D. Tuan, A. A. Nasir, T. Q. Duong, and H. V. Poor, "Power allocation for energy efficiency and secrecy of wireless interference networks," *IEEE Trans. Wirel. Commun.*, 2018 (Early Access).